Long-term potentiation in rat hippocampal neurons is accompanied by spatially widespread changes in intrinsic oscillatory dynamics and excitability

Rishikesh Narayanan and Daniel Johnston

Neuron, 56, 2007

SUPPLEMENTAL FIGURES

(Contains 14 supplemental figures with each of them followed by the corresponding legend)

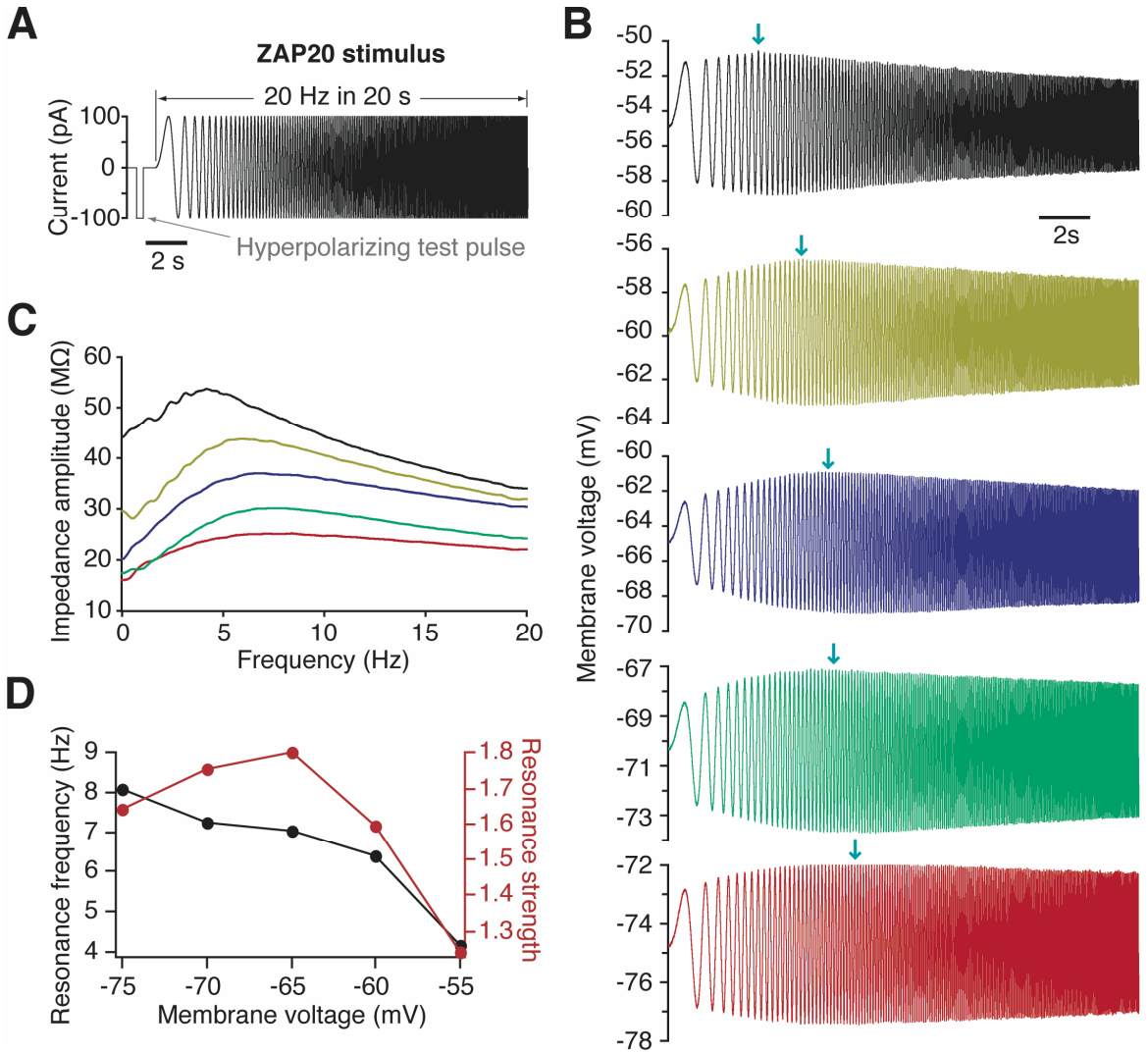
A
ZAP20 stimulus
20 Hz in 20 s
Current (pA)
100
0
-100
2 s
Hyperpolarizing test pulse
B
Membrane voltage (mV)
2s
C
Impedance amplitude (MΩ)
Frequency (Hz)
D
Resonance frequency (Hz)
Resonance strength
Membrane voltage (mV)

Figure S1. Illustration of voltage dependence of the impedance amplitude profile (ZAP) (A) ZAP20 stimulus used in all characterization experiments consists of a 100 pA hyperpolarizing pulse followed by a constant amplitude sinusoid with frequency linearly spanning 0–20 Hz in 20 s. The peak-to-peak amplitude of the sinusoid is set at 200 pA for measurements made at hyperpolarized voltages and is reduced for measurements at depolarized voltages, in order to avoid spikes. (B) Responses of a CA1 pyramidal cell dendrite 270 μm away from the soma to the ZAP20 stimulus injection (the response to the hyperpolarizing pulse is not shown). Each panel shows the response of the dendrite measured at different membrane voltages, which were set by injecting appropriate depolarizing or hyperpolarizing holding current. Arrows indicate the location of maximal response in each trace. A progressive rightward shift in this maximal response location is observed with hyperpolarization of membrane voltage. (C) Impedance amplitude profile obtained for each of the subpanels in (B), color-coded corresponding to subpanels in (B). (D) Resonance frequency and resonance strength, obtained from (C), plotted as a function of membrane voltage reveals an increase in both parameters with hyperpolarization.

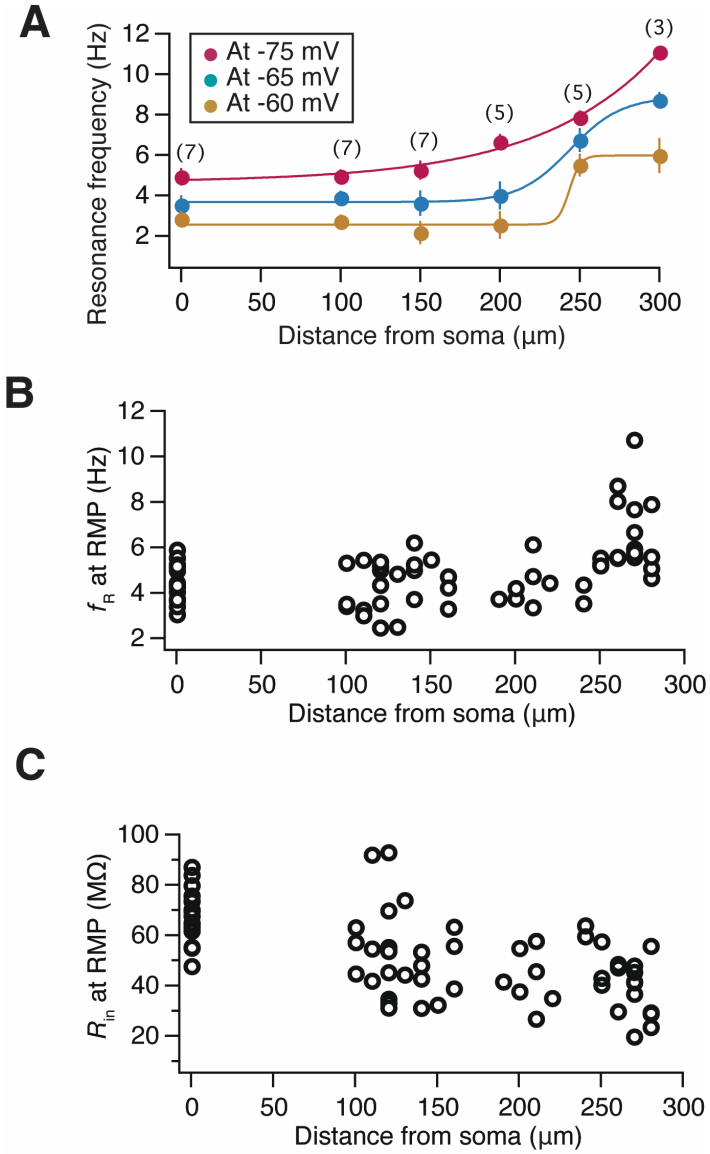
A
Resonance frequency (Hz)
At -75 mV
At -65 mV
At -60 mV
(7)
(7)
(7)
(5)
(5)
(3)
Distance from soma (μm)
B
f_R at RMP (Hz)
Distance from soma (μm)
C
R_{in} at RMP (MΩ)
Distance from soma (μm)

Figure S2. (A) Resonance frequency of dendrites increases with distance from the soma (data same as Fig. 1B). Markers (●: measured at -75 mV; ●: measured at -65 mV; ●: measured at -60 mV) correspond to experimental values, and solid lines indicate sigmoidal fits (functional form $(1 + \exp((x_{1/2} - x)/\kappa))^{-1}$, **-75 mV:** $x_{1/2}$ = 370.7 µm; κ = 62.19 µm; χ^2 = 0.20; **-65 mV:** $x_{1/2}$ = 244.1 µm; κ = 16.18 µm; χ^2 = 0.07; **-60 mV**: $x_{1/2}$ = 243.6 µm; κ = 3.5 µm; χ^2 = 0.26) to respective experimental values. It may be noted that at around rest (-65 mV to -60 mV), the dendritic resonance frequency remains constant up to around 250 µm, with a distinct jump beyond that. This is quantitatively substantiated by the sigmoidal fits. The number within parenthesis at each distance value is the number of somatic (zero distance) or dendritic recordings (at that distance). (B) Baseline scatter plot of resonance frequency measured at corresponding resting membrane potentials (RMP) along the distance of the somato-apical trunk. It may be noted that, at rest, the resonance frequency remains almost constant up to around 250 µm, with a steep increase beyond that. This conforms to measurements performed at -65 mV and -60 mV (A), and the sigmoidal fit shown in (A). (C) Baseline scatter plot of input resistance measured at corresponding resting membrane potentials along the distance of the somato-apical trunk. It may be noted that input resistance reduces with distance, conforming to data presented in Fig. 1G. (B–C) were obtained from recordings performed as part of the ATBF and ATBP experiments (Fig. 4&5).

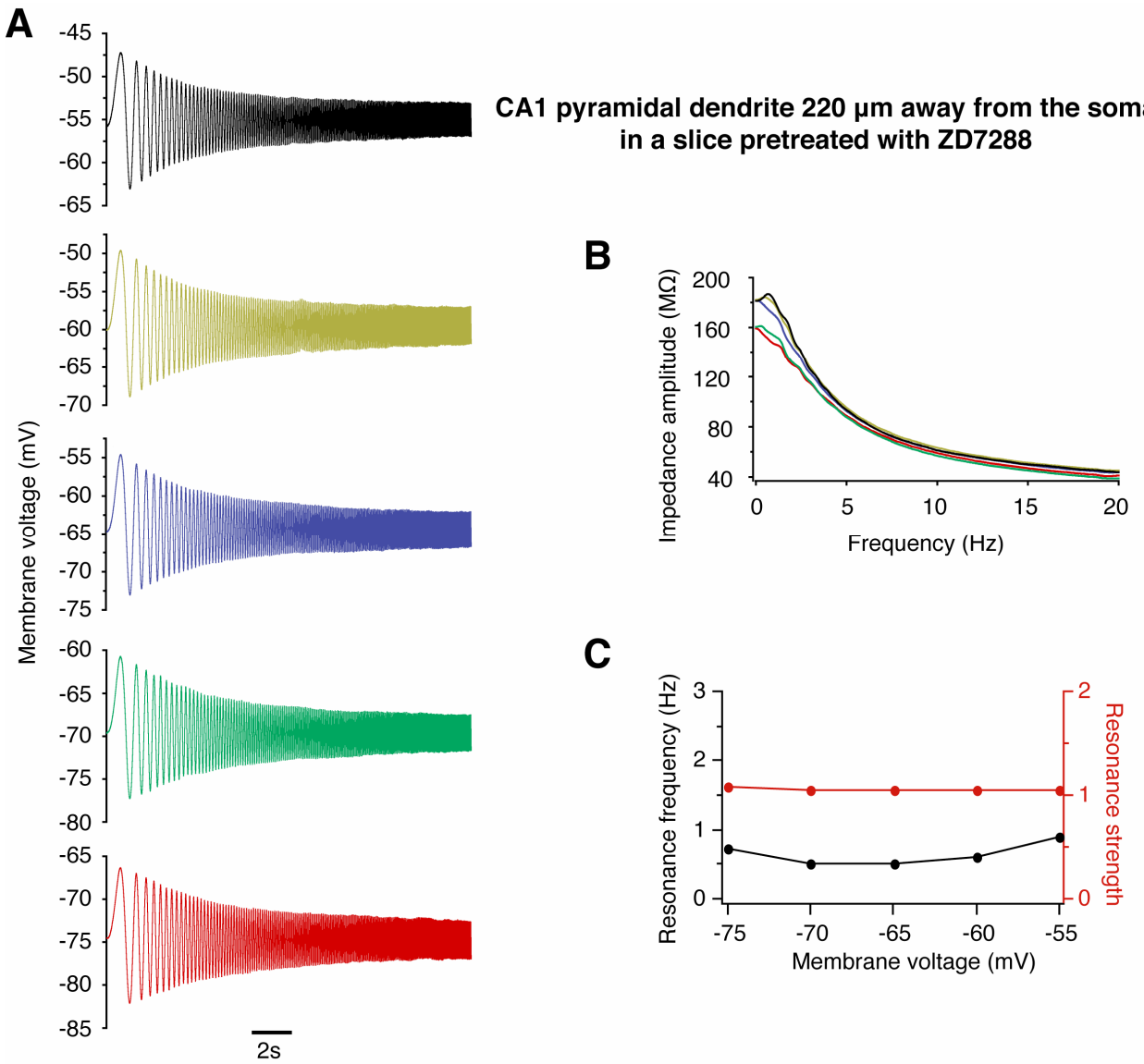
A
CA1 pyramidal dendrite 220 µm away from the soma
in a slice pretreated with ZD7288
Membrane voltage (mV)
-45
-50
-55
-60
-65
-50
-55
-60
-65
-70
-55
-60
-65
-70
-75
-60
-65
-70
-75
-80
-65
-70
-75
-80
-85
2s
B
Impedance amplitude (MΩ)
200
160
120
80
40
0
5
10
15
20
Frequency (Hz)
C
Resonance frequency (Hz)
3
2
1
0
2
1
0
Resonance strength
-75
-70
-65
-60
-55
Membrane voltage (mV)

Figure S3. Example impedance amplitude profiles obtained from a dendrite in slices pretreated with 100 μM ZD7288. We pretreated slices for five minutes with 100 μM ZD7288 and assessed resonance properties without adding ZD7288 to the recording solutions, because ZD7288 irreversibly blocks the I_h current (Gasparini and Difrancesco, Pflugers Arch. 435(1), 1997) (A) Responses of a CA1 pyramidal cell dendrite 220 μm away from the soma to the ZAP20 stimulus injection (Fig. S1A; the response to the hyperpolarizing pulse is not shown). Each panel shows the response of the dendrite measured at different membrane voltages, which were set by injecting appropriate depolarizing or hyperpolarizing holding current. (B) Impedance amplitude profile obtained for each of the subpanels in (A), color-coded corresponding to subpanels in (A). In each plot, it may be noted that the impedance amplitude monotonically decreases with increase in frequency, reminiscent of a passive cable. This may be contrasted with the profiles shown in (Fig. S1B) to observe that resonance is abolished by ZD7288 pretreatment in this voltage range (-75 mV to -55 mV). (C) Resonance frequency and resonance strength, obtained from (B), plotted as a function of membrane voltage quantitatively brings out the abolishment of resonance by ZD7288.

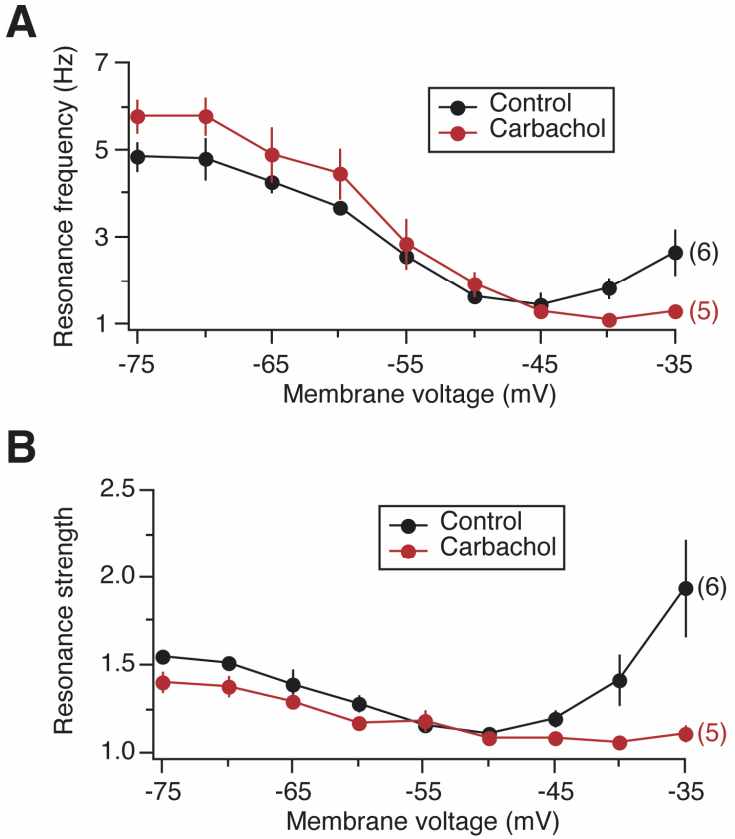
A
Resonance frequency (Hz)
7
5
3
1
Control
Carbachol
(6)
(5)
-75
-65
-55
-45
-35
Membrane voltage (mV)
B
Resonance strength
2.5
2.0
1.5
1.0
Control
Carbachol
(6)
(5)
-75
-65
-55
-45
-35
Membrane voltage (mV)

Figure S4. Confirmation of the presence of two forms of resonance in CA1 pyramidal cells (Hu et al., 2002), one at hyperpolarized voltages mediated by I_h, and the other at more depolarized voltages mediated by I_M. Whole-cell patch-clamp recordings from CA1 pyramidal cell soma were performed in the presence of 10 μM CNQX, 10 μM (+)bicuculline, 10 μM picrotoxin, 50 μM D, L-APV, 2 μM CGP55845, 1 μM TTX and 2 mM $NiCl_2$. The increase in resonance frequency (A) and resonance strength (B) in the hyperpolarized voltage range (-75 mV to -55 mV; Control, ●) is consistent with data presented in (Fig. 1), and is mediated by I_h in the soma (Fig. 2 and Hu et al., 2002) and dendrites (Fig. 2). Increase in resonance frequency (A) and resonance strength (B) in depolarized voltages (-50 mV to -35 mV; Control, ●) is dependent on I_M, as 10 μM Carbachol, a muscarinic agonist, in the bath abolishes resonance in that voltage range, affecting neither resonance frequency nor resonance strength in hyperpolarized voltages (Carbachol, ●). Numbers within parentheses indicate the number of cells assessed for each of the two populations (Control and Carbachol).

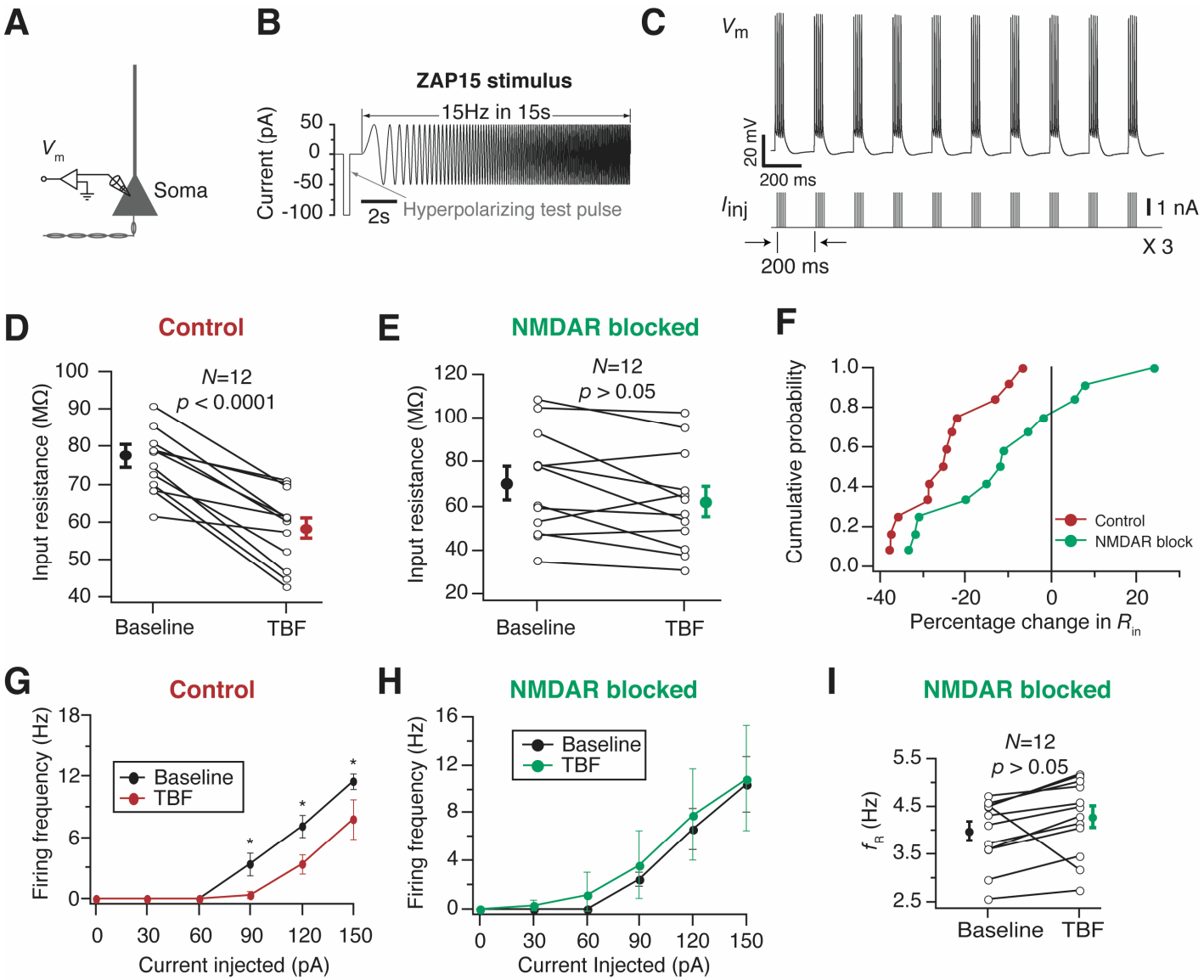
A
B
C
V_m
Soma
ZAP15 stimulus
15Hz in 15s
Current (pA)
50
0
-50
-100
2s
Hyperpolarizing test pulse
V_m
20 mV
200 ms
I_{inj}
1 nA
X 3
200 ms
D
Control
N=12
p < 0.0001
Input resistance (MΩ)
Baseline
TBF
E
NMDAR blocked
N=12
p > 0.05
Input resistance (MΩ)
Baseline
TBF
F
Cumulative probability
Control
NMDAR block
Percentage change in R_{in}
G
Control
Firing frequency (Hz)
Baseline
TBF
Current injected (pA)
H
NMDAR blocked
Firing frequency (Hz)
Baseline
TBF
Current Injected (pA)
I
NMDAR blocked
N=12
p > 0.05
f_R (Hz)
Baseline
TBF

Figure S5. Theta burst firing (TBF) results in an NMDAR-dependent reduction in excitability (confirmation of Fan et al., 2005) and increase in resonance frequency. (A) Schematic of the somato-apical trunk depicting the experimental design for assessing activity-dependent plasticity in excitability and resonance properties of the soma. Voltage responses of the soma were recorded using a whole-cell patch-clamp electrode (V_m). (B) ZAP15 stimulus, used in all plasticity experiments, consists of a 100 pA hyperpolarizing pulse followed by a constant amplitude sinusoid with its frequency linearly spanning 0-15 Hz in 15 s. The constant peak-to-peak amplitude was always set at 100 pA for all plasticity experiments. (C) Induction of plasticity is carried out by theta burst firing elicited by somatic current injections (I_{inj}). Example responses of soma (top, V_m) to TBF stimulus (bottom, I_{inj}) are shown along with the pattern of current injections. (D) Population data of input resistance (R_{in}) measured before (Baseline; ●) and 40 minutes after TBF (TBF; ●) reveals a significant reduction (paired *Student's t* test; **Baseline:** 76.95 ± 3.05 MΩ; **TBF:** 57.94 ± 2.83 MΩ) after TBF. (E) In TBF experiments performed in the presence of N-Methyl D-Aspartate receptor (NMDAR) antagonists (50 µM D, L-APV and 10 µM (+)MK801), population data of input resistance (R_{in}) measured before (Baseline; ●) and 40 minutes after TBF (TBF; ●) demonstrate the requirement of NMDAR for TBF-induced reduction in input resistance (*p* value corresponds to paired *Student's t* test; **Baseline:** 70.15 ± 7.49 MΩ; **TBF:** 62.10 ± 7.13 MΩ) after TBF. (F) Cumulative probability plot of data in (D) and (E). Each point represents the magnitude of change, at 40 minutes after TBF, relative to respective baseline in control (●) or NMDAR block (●) experiments. It may be noted that the plots are non-overlapping. (G) Population plots of action potential firing frequency as a function of injected current to the soma bring out significant reductions after TBF (Baseline: ●; 40 min after TBF: ●). *: $p<0.05$, paired *Student's t* test. (H) TBF-induced reduction in action potential firing frequency is blocked (Baseline: ●; 40 min after TBF: ●) when TBF experiments were conducted in the presence of NMDAR antagonists. (I) In TBF experiments performed in the presence of NMDAR antagonists, population data of resonance frequency (f_R) measured before (Baseline; ●) and 40 minutes after TBF (TBF; ●) establish the requirement of NMDARs for TBF-induced increase in resonance frequency (*p* value corresponds to paired *Student's t* test, **Baseline:** 3.97 ± 0.19 Hz; **TBF:** 4.27 ± 0.22 Hz). After TBF, resonance strength (Q) values were significantly different from their baseline values in the control group (Baseline: 1.32 ± 0.03; TBF: 1.40 ± 0.02. $p<0.01$, paired *Student's t*-test), but not in the "NMDAR Block" group (Baseline: 1.25 ± 0.03; TBF: 1.27 ± 0.04. $p>0.5$, paired *Student's t*-test). After TBF, sag ratio values were significantly different from their respective baseline values in the control group (Baseline: 22.20 ± 1.29; TBF: 24.92 ± 0.83. $p<0.05$, paired *Student's t*-test), but not in the "NMDAR Block" group (Baseline: 20.78 ± 1.38; TBF: 22.47 ± 1.16. $p>0.4$, paired *Student's t*-test). TBF-induced depolarizing shift to resting membrane potential was 3.24 ± 0.68 mV ($p<0.01$; paired *Student's t* test) which was blocked (0.14 ± 0.35 mV shift; $p>0.5$) in experiments in the presence of NMDAR antagonists.

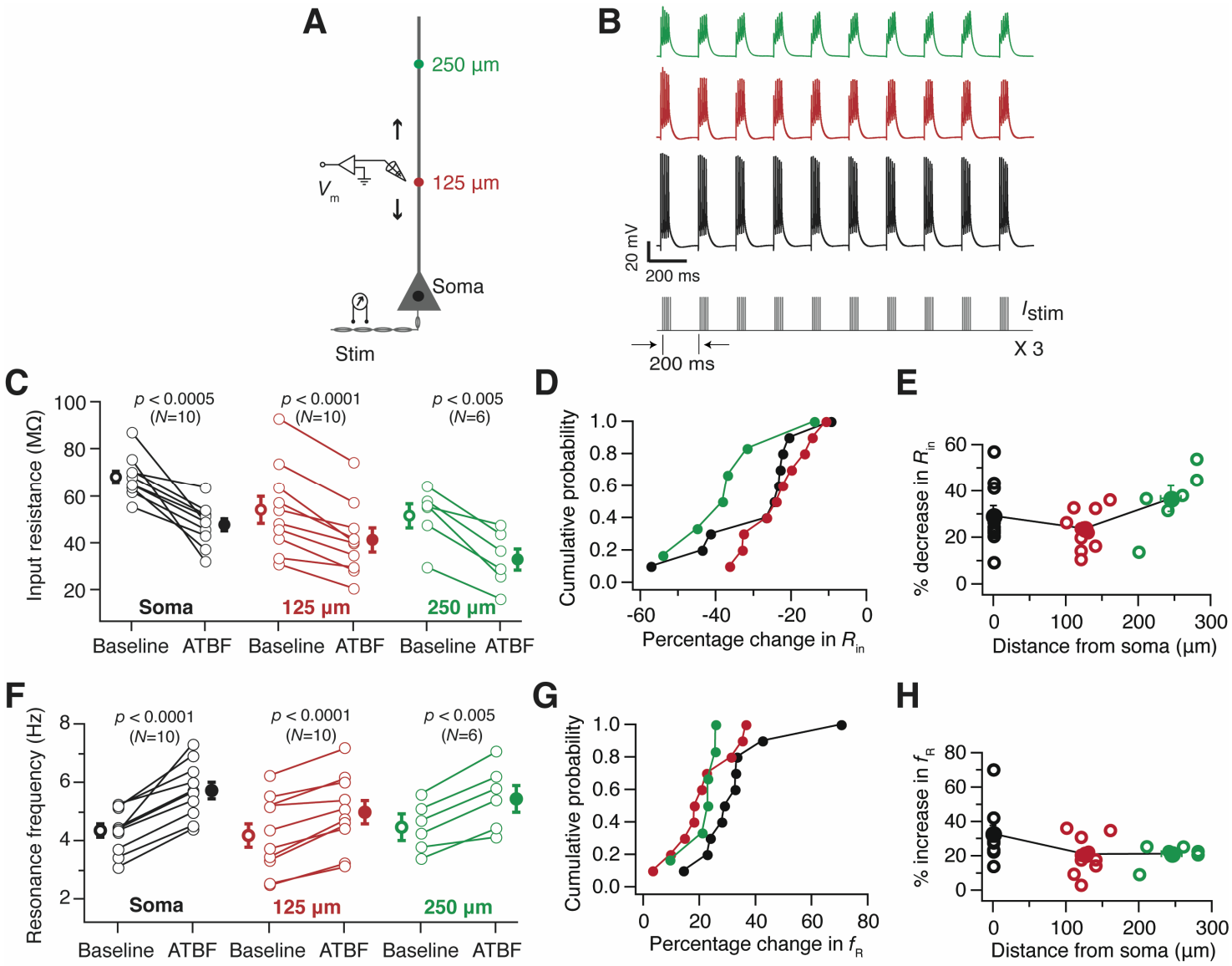
A
250 µm
125 µm
V_m
Soma
Stim
B
20 mV
200 ms
I_{stim}
200 ms
X 3
C
Input resistance (MΩ)
p < 0.0005 (N=10)
p < 0.0001 (N=10)
p < 0.005 (N=6)
Soma
125 µm
250 µm
Baseline ATBF Baseline ATBF Baseline ATBF
D
Cumulative probability
Percentage change in R_{in}
E
% decrease in R_{in}
Distance from soma (µm)
F
Resonance frequency (Hz)
p < 0.0001 (N=10)
p < 0.0001 (N=10)
p < 0.005 (N=6)
Soma
125 µm
250 µm
Baseline ATBF Baseline ATBF Baseline ATBF
G
Cumulative probability
Percentage change in f_R
H
% increase in f_R
Distance from soma (µm)

Figure S6. (A) Schematic of the somato-apical trunk depicting the experimental design for assessing activity-dependent plasticity in excitability and resonance properties as functions of distance from the soma. Voltage responses of the soma and dendrites at various distances (up to around 300 µm from the soma) were recorded locally using a whole-cell patch-clamp electrode (V_m). Induction of plasticity is carried out by theta burst firing elicited by antidromic stimulation (Stim). Recordings along the somato-apical trunk are binned into three subpopulations (Soma, 125 µm, and 250 µm) depending on the distance of the recording location from the soma. Colors of markers along the somato-apical trunk serve as codes for corresponding distances in (B–H). (B) Example responses of soma (black), and dendrites located at 140 µm (red) and 240 µm (green) to ATBF stimulus pattern shown below (I_{stim}). It may be noted that the backpropagating action potential amplitude reduces with increasing distance from the soma. (C–E) ATBF elicits near-identical reduction in input resistance (R_{in}) across the dendritic tree. (C) Population plots of R_{in} measured before (Baseline; open circles) and 40 minutes after ATBF (ATBF; solid circles) represented as three different populations show a significant reduction (paired *Student's t* test; **Soma:** Baseline: 68.2 ± 2.7 MΩ, ATBF: 47.74 ± 2.78 MΩ; **125 µm:** Recording distance: 126 ± 5.42 µm, Baseline: 54.28 ± 5.99 MΩ, ATBF: 41.48 ± 4.89 MΩ; **250 µm:** Recording distance: 245 ± 14.08 µm, Baseline: 51.71 ± 4.93 MΩ, ATBF: 33.18 ± 4.78 MΩ) after ATBF. (D) Cumulative probability plot of data in (C). Each point represents change in R_{in} at 40 minutes after ATBF, relative to respective baseline values in populations of soma (●), dendrites around 125 µm (●), and dendrites around 250 µm (●). (E) Scatter plot of data in (C). Each open circle represents the magnitude of change, at 40 minutes after ATBF, relative to the respective baseline value of R_{in} in a given experiment. The solid circles represent the average distance and average plasticity for the three populations. Percentage reduction in R_{in} at 40 min after ATBF: **Soma:** 29.22 ± 4.41, **125 µm:** 23.66 ± 2.69, **250 µm:** 36.65 ± 5.53. (F-H) ATBF elicits near-identical increase in resonance frequency (f_R) across the dendritic tree. (F) Population plots of f_R measured before (Baseline; open circles) and 40 minutes after ATBF (ATBF; solid circles) represented as three different populations show a significant increase (paired *Student's t* test; **Soma:** Baseline: 4.34 ± 0.24 Hz, ATBF: 5.72 ± 0.30 Hz; **125 µm:** Baseline: 4.2 ± 0.41 Hz, ATBF: 4.99 ± 0.40 Hz; **250 µm:** Baseline: 4.49 ± 0.45 Hz, ATBF: 5.46 ± 0.46 Hz) after ATBF. The resonance frequency values shown here do not have a significant increase in the 250 µm case. The apparent discrepancy arises because it was difficult to do the longer duration experiments while recording from dendrites greater than about 250 µm from the soma, which is where the significant increase in resonance frequency is most obvious. However, we have plotted the baseline resonance frequency (Fig. S2B) and input resistance (Fig. S2C) values obtained with all ATBP and ATBF experiments (including the more distal dendrites that did not survive through the long duration experiments, and hence not used for other analyses). It may be noted that there is a distinct jump in resonance frequency beyond 250 µm away from the soma (Fig. S2B). (G) Cumulative probability plot of data in (C). Each point represents change in f_R at 40 minutes after ATBF, relative to respective baseline values in populations of soma (●), dendrites around 125 µm (●), and dendrites around 250 µm (●). Overlapping cumulative plots corresponding to all three populations, confirm that activity-dependent changes in input resistance (D) and resonance frequency (G) are near identical across the dendritic tree. (H) Scatter

plot of data in (F). Notations are similar to (E). Percentage increase in f_R at 40 min after ATBF: **Soma:** 32.90 ± 4.802, **125 µm:** 20.96 ± 3.42, **250 µm:** 21.25 ± 2.48. After ATBF, resonance strength (Q) values were significantly different from their respective baseline values in all three populations (**Soma:** Baseline: 1.19 ± 0.03; ATBF: 1.31 ± 0.02. $p<0.01$, **125 µm:** Baseline: 1.28 ± 0.05; ATBF: 1.43 ± 0.05. $p<0.001$, **250 µm:** Baseline: 1.28 ± 0.45; ATBF: 1.50 ± 0.46. $p<0.01$, paired *Student's t*-test). After ATBF, sag ratio values were significantly different from their respective baseline values in all three populations (**Soma:** Baseline: 19.89 ± 1.18; ATBF: 23.83 ± 0.73. $p<0.01$, **125 µm:** Baseline: 24.76 ± 1.58; ATBF: 28.35 ± 0.97. $p<0.01$, **250 µm:** Baseline: 26.90 ± 0.45; ATBF: 33.67 ± 0.461. $p<0.01$, paired *Student's t*-test). ATBF-induced depolarizing shifts to resting membrane potential across the three populations were **Soma:** 3.65 ± 0.48 mV, **125 µm:** 2.80 ± 0.31 mV, **250 µm:** 3.35 ± 0.45 mV ($p<0.001$ for all cases; paired *Student's t* test).

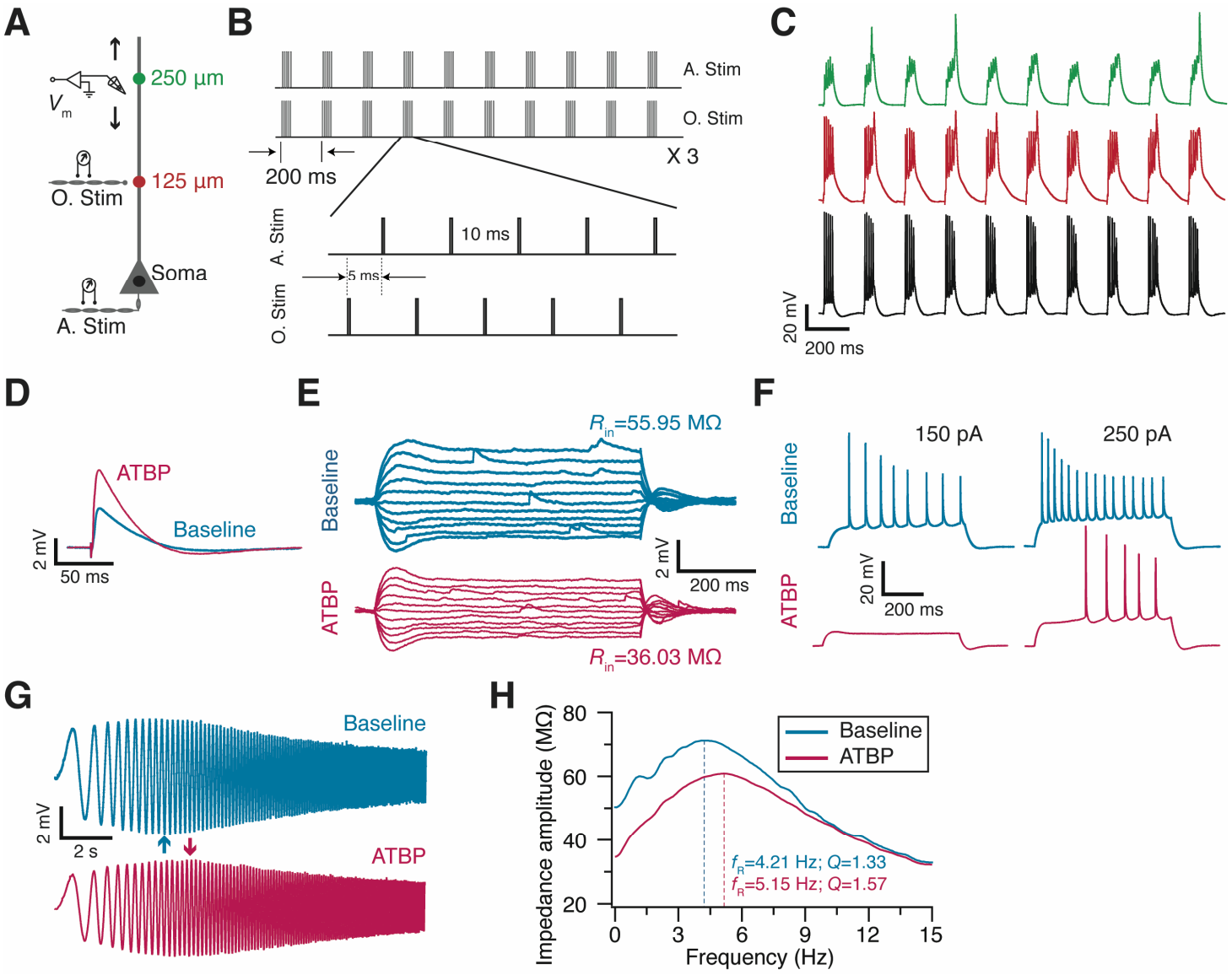
A
250 µm
V_m
125 µm
O. Stim
Soma
A. Stim
B
A. Stim
O. Stim
X 3
200 ms
10 ms
5 ms
C
20 mV
200 ms
D
ATBP
Baseline
2 mV
50 ms
E
R_{in}=55.95 MΩ
Baseline
2 mV
200 ms
ATBP
R_{in}=36.03 MΩ
F
150 pA
250 pA
Baseline
20 mV
200 ms
ATBP
G
Baseline
2 mV
2 s
ATBP
H
Impedance amplitude (MΩ)
80
60
40
20
Baseline
ATBP
f_R=4.21 Hz; Q=1.33
f_R=5.15 Hz; Q=1.57
0
3
6
9
12
15
Frequency (Hz)

Figure S7. (A) Schematic of the somato-apical trunk depicting the experimental design for assessing LTP-associated plasticity in excitability and resonance properties as functions of distance from the soma. Voltage responses of the soma and dendrites at various distances (up to around 300 µm from the soma) were recorded locally using a whole-cell patch-clamp electrode (V_m). EPSPs were elicited by stimulating the orthodromic pathway (O. Stim) located at around 125 µm from the soma, irrespective of location of the recording electrode. Recordings along the somato-apical trunk are binned into three subpopulations (Soma, 125 µm, and 250 µm) depending on the distance of the recording location from the soma. Colors of markers along the somato-apical trunk serve as codes for corresponding distances in (C). (B) Induction of LTP is carried out by theta burst pairing of antidromic stimulation (A. Stim) and orthodromic stimulation (O. Stim). Within a burst, orthodromic stimulation precedes antidromic stimulation by 5 ms. The shift is set at 5 ms in order to match the peaks of the antidromically initiated action potential and the orthodromically initiated EPSP in a dendrite located around 125 µm. Irrespective of the location of the recording electrode, the same induction protocol is used, given that the orthodromic stimulating electrode is always located at around 125 µm. The locations of stimulating electrode for the three recording locations are 130 ± 6.2 µm (soma), 118.3 ± 9.1 µm (125 µm) and 126.6 ± 11.4 µm (250 µm). They are not significantly different from each other (p>0.5; one-way *ANOVA*). (C) Example responses of soma (black), and dendrites located at 140 µm (red) and 270 µm (green) to ATBP induction protocol (B). It may be noted that the backpropagating action potential amplitude reduces with increasing distance from the soma. (D)–(H) Typical ATBP experiment in a dendrite located at 160 µm away from the soma and the orthodromic stimulating electrode located at 110 µm away from the soma. (D) Typical EPSPs recorded before (Baseline) and 40 minutes after ATBP (ATBP) show an increase in amplitude and slope of the EPSP, indicating LTP of synaptic response. (E) Responses of the cell to constant current pulses of 700 ms duration, varying in amplitude from -50 pA to +50 pA before (Baseline) and 40 minutes after ATBP (ATBP). Input resistance (R_{in}), measured as the slope of the V–I curve obtained from steady-state voltage deflections for each of this curves, reduces after ATBP. (F) Example voltage traces recorded by injecting 150 pA (left) and 250 pA (right) depolarizing current locally to the dendrite before (Baseline) and 40 minutes after ATBP (ATBP) bring out a significant reduction in the number of action potentials fired after ATBP. (G) Response of the neuron to the ZAP15 stimulus (Fig. S5B) during the baseline period (Baseline), and 40 minutes after ATBP (ATBP). Arrows in corresponding colors indicate the location of maximal response in each trace. It may be noted that the location of maximal response is shifted to the right in the ATBP trace with respect to that in the baseline trace, indicating an increase in resonance frequency. (H) Impedance amplitude as a function of frequency computed from correspondingly color-coded traces in (G). It may be noted that 40 minutes after ATBP, there is an increase in resonance frequency (compare dotted lines) and resonance strength with respect to their baseline values.

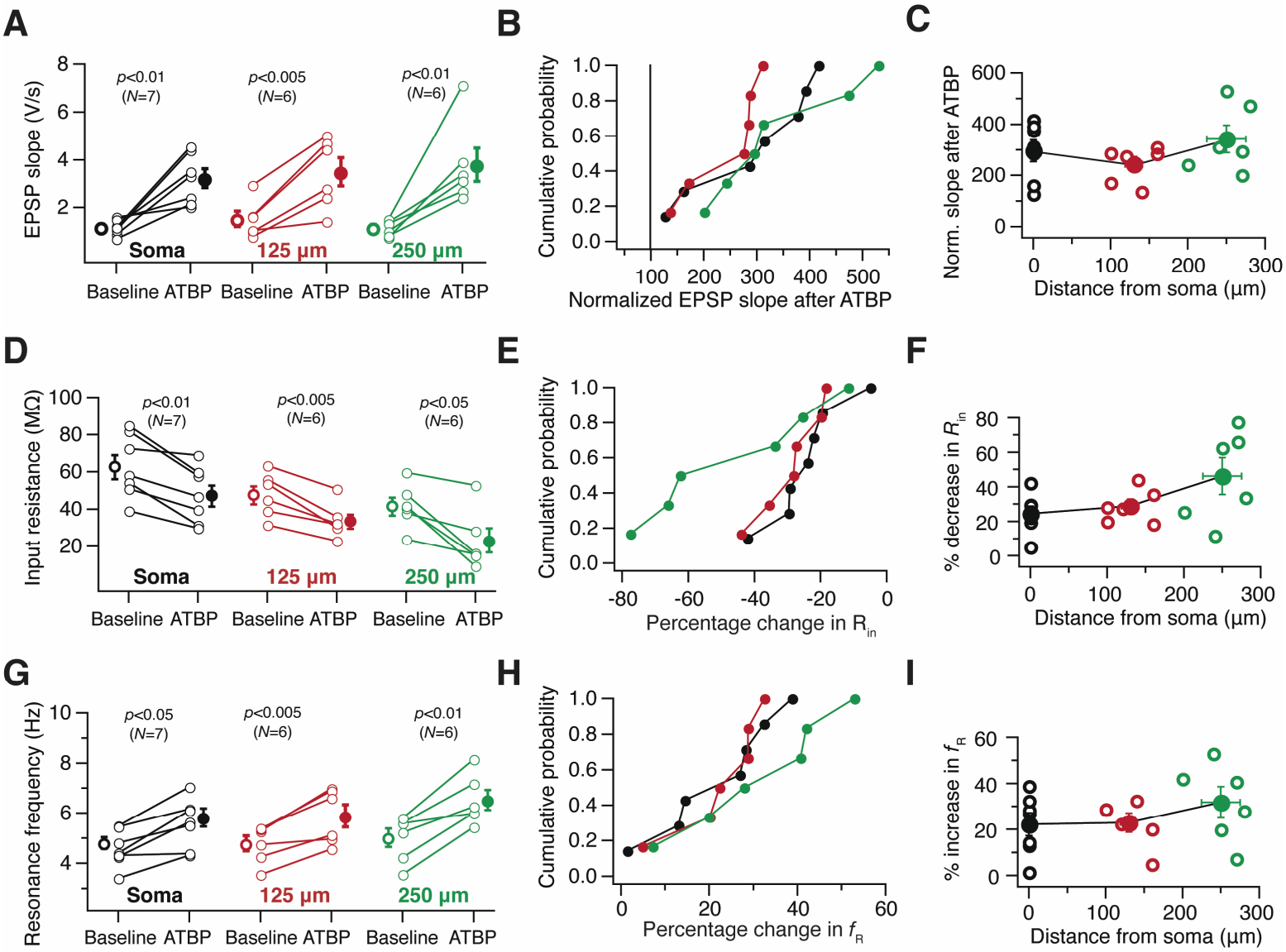
A
EPSP slope (V/s)
p<0.01 (N=7)
p<0.005 (N=6)
p<0.01 (N=6)
Soma
125 µm
250 µm
Baseline ATBP Baseline ATBP Baseline ATBP
B
Cumulative probability
Normalized EPSP slope after ATBP
C
Norm. slope after ATBP
Distance from soma (µm)
D
Input resistance (MΩ)
p<0.01 (N=7)
p<0.005 (N=6)
p<0.05 (N=6)
Soma
125 µm
250 µm
Baseline ATBP Baseline ATBP Baseline ATBP
E
Cumulative probability
Percentage change in R_in
F
% decrease in R_in
Distance from soma (µm)
G
Resonance frequency (Hz)
p<0.05 (N=7)
p<0.005 (N=6)
p<0.01 (N=6)
Soma
125 µm
250 µm
Baseline ATBP Baseline ATBP Baseline ATBP
H
Cumulative probability
Percentage change in f_R
I
% increase in f_R
Distance from soma (µm)

Figure S8. LTP is accompanied by a reduction in input resistance and an increase in resonance frequency across the somato-apical trunk. Experimental design and color code are given in Fig. S7A. (A) Population plots of EPSP slope measured before (Baseline; open circles) and 40 minutes after ATBP (ATBP; solid circles) represented as three different populations show a significant increase (paired *Student's t* test; **Soma:** Baseline: 1.15 ± 0.12 V/s, ATBP: 3.18 ± 0.39 V/s; **125 µm:** Recording distance: 130 ± 11.25 µm, Baseline: 1.49 ± 0.32 V/s, ATBP: 3.45 ± 0.59 V/s; **250 µm:** Recording distance: 250 ± 25.16 µm, Baseline: 1.12 ± 0.13 V/s, ATBP: 3.75 ± 0.70 V/s) after ATBP. (B) Cumulative probability plot of data in (A). Each point represents average EPSP slope computed at 35–40 minutes after ATBP, normalized with respect to respective baseline values (computed over the five minute baseline period) in populations of soma (●), dendrites around 125 µm (●), and dendrites around 250 µm (●). (C) Scatter plot of data in (A). Each open circle represents the magnitude of change, at 35–40 minutes after ATBP, relative to the respective baseline value of EPSP slope in a given experiment. The solid circles represent the average distance and average plasticity for the three populations. Normalized EPSP slope at 35–40 min after ATBP: **Soma:** 296.24 ± 43.08, **125 µm:** 244.25 ± 29.41, **250 µm:** 342.32 ± 53.46. (D) Population plots of R_{in} measured before (Baseline; open circles) and 40 minutes after ATBP (ATBP; solid circles) represented as three different populations show a significant reduction (paired *Student's t* test; **Soma:** Baseline: 63.15 ± 6.43 MΩ, ATBP: 47.76 ± 5.67 MΩ; **125 µm:** Baseline: 48.08 ± 4.81 MΩ, ATBP: 33.97 ± 3.80 MΩ; **250 µm:** Baseline: 41.96 ± 4.84 MΩ, ATBP: 22.93 ± 6.47 MΩ) after ATBP. (E) Cumulative probability plot of data in (D). Each point represents change in R_{in} at 40 minutes after ATBP, relative to respective baseline values in populations of soma (●), dendrites around 125 µm (●), and dendrites around 250 µm (●). (F) Scatter plot of data in (D). Notations similar to (C). Percentage reduction in R_{in} at 40 min after ATBP: **Soma:** 24.52 ± 4.29, **125 µm:** 28.91 ± 3.95, **250 µm:** 46.18 ± 10.67. (G) Population plots of resonance frequency (f_R) measured before (Baseline; open circles) and 40 minutes after ATBP (ATBP; solid circles) represented as three different populations show a significant increase (paired *Student's t* test; **Soma:** Baseline: 4.78 ± 0.23 Hz, ATBP: 5.80 ± 0.36 Hz; **125 µm:** Baseline: 4.76 ± 0.30 Hz, ATBP: 5.85 ± 0.44 Hz; **250 µm:** Baseline: 5 ± 0.36 Hz, ATBP: 6.50 ± 0.40 Hz) after ATBP. The resonance frequency values shown here do not have a significant increase in the 250 µm case. The apparent discrepancy arises because it was difficult to do the longer duration experiments while recording from dendrites greater than about 250 µm from the soma, which is where the significant increase in resonance frequency is most obvious. However, we have plotted the baseline resonance frequency (Fig. S2B) and input resistance (Fig. S2C) values obtained with all ATBP and ATBF experiments (including the more distal dendrites that did not survive through the long duration experiments, and hence not used for other analyses). It may be noted that there is a distinct jump in resonance frequency beyond 250 µm away from the soma (Fig. S2B). (H) Cumulative probability plot of data in (G). Notations similar to (B). Overlapping cumulative plots corresponding to all three populations, confirm that LTP-associated changes in input resistance (E) and resonance frequency (H) are near identical across the dendritic tree. (I) Scatter plot of data in (G). Notations are similar to (C). Percentage increase in f_R at 40 min after ATBP: **Soma:** 22.19 ± 4.91, **125 µm:** 22.88 ± 4.06, **250 µm:** 31.76 ± 6.81. After ATBP, resonance strength (Q) values were significantly different

from their respective baseline values in all three populations (**Soma:** Baseline: 1.23 ± 0.05; ATBP: 1.36 ± 0.06. $p<0.01$, **125 µm:** Baseline: 1.39 ± 0.04; ATBP: 1.57 ± 0.05. $p<0.01$, **250 µm:** Baseline: 1.26 ± 0.03; ATBP: 1.94 ± 0.23. $p<0.05$, paired *Student's t*-test). After ATBP, sag ratio values were significantly different from their respective baseline values in all three populations (**Soma:** Baseline: 21.66 ± 1.63; ATBP: 24.98 ± 1.63. $p<0.01$, **125 µm:** Baseline: 30.85 ± 1.51; ATBP: 35.73 ± 1.93. $p<0.01$, **250 µm:** Baseline: 25.79 ± 2.19; ATBP: 40.00 ± 4.49. $p<0.01$, paired *Student's t*-test). ATBP-induced depolarizing shifts to resting membrane potential across the three populations were **Soma:** 2.76 ± 0.81 mV, **125 µm:** 4.59 ± 0.37 mV, **250 µm:** 3.57 ± 0.76 mV ($p<0.001$ for all cases; paired *Student's t* test).

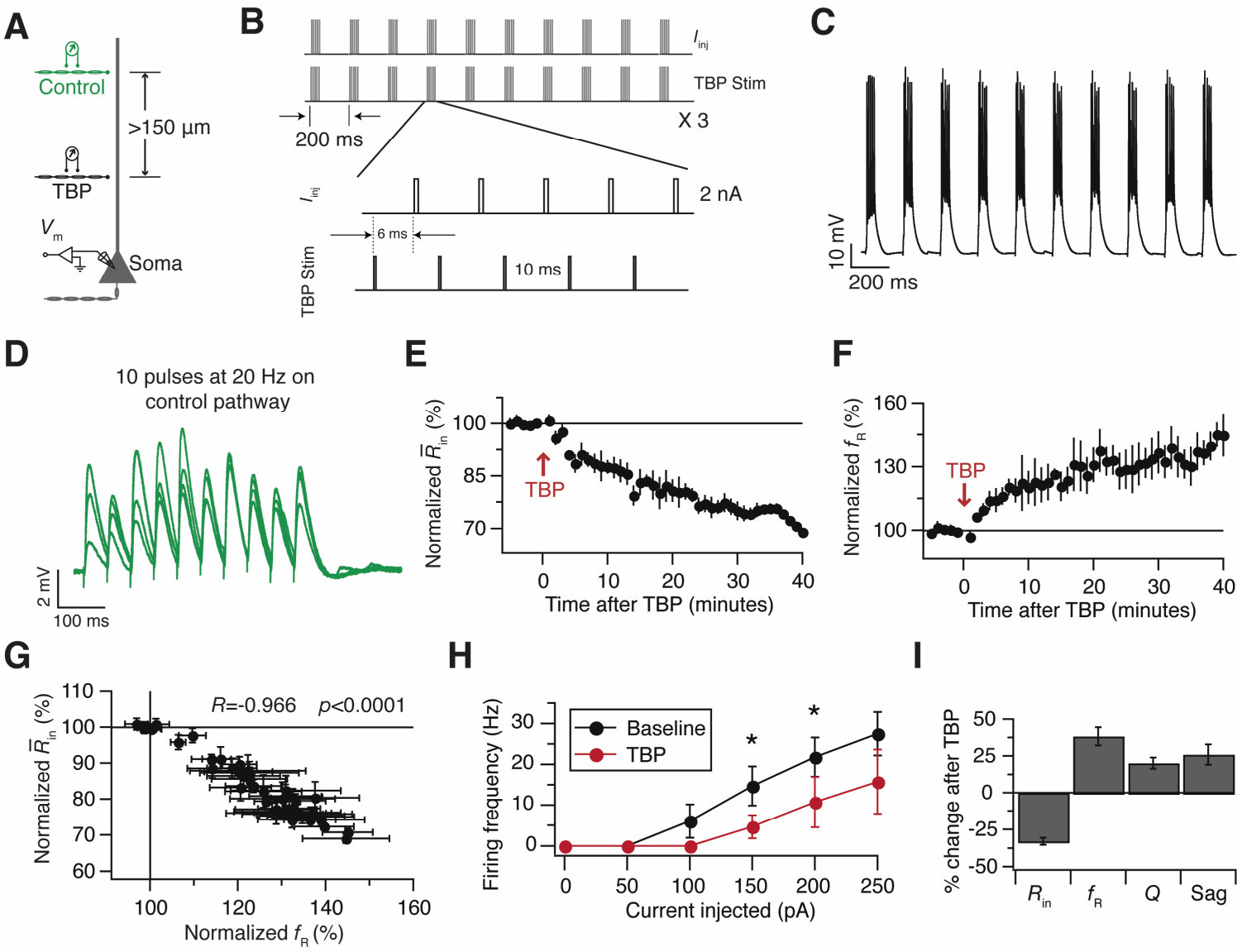
A
Control
>150 µm
TBP
V_m
Soma
B
I_{inj}
TBP Stim
X 3
200 ms
2 nA
6 ms
10 ms
C
10 mV
200 ms
D
10 pulses at 20 Hz on control pathway
2 mV
100 ms
E
Normalized $\bar{R}_{in}$ (%)
TBP
Time after TBP (minutes)
F
Normalized f_R (%)
TBP
Time after TBP (minutes)
G
R=-0.966 p<0.0001
Normalized $\bar{R}_{in}$ (%)
Normalized f_R (%)
H
Baseline
TBP
Firing frequency (Hz)
Current injected (pA)
I
% change after TBP
R_{in}
f_R
Q
Sag

Figure S9. (A) Schematic of the somato-apical trunk depicting the experimental design for assessing LTP-associated plasticity in evoked temporal summation. Voltage responses of the soma were recorded using a whole-cell patch-clamp electrode (V_m). EPSPs were elicited by stimulating either the Control pathway (Control) or the TBP pathway (TBP). The TBP pathway is located at 115 ± 4.28 µm from the soma, and the Control stimulating electrode is at 283 ± 3.33 µm from the soma. (B) Induction of LTP is carried out by theta burst pairing of somatically induced spikes (represented as I_{inj}; each pulse typically is 2 nA for 2 ms) and orthodromic stimulation along the TBP pathway (TBP). Within a burst, orthodromic stimulation precedes antidromic stimulation by 6 ms. The shift is set at 6 ms in order to match the peaks of the antidromically initiated action potential and the orthodromically initiated EPSP in a dendrite located around 125 µm. The 1 ms addition to this time-shift in comparison to the ATBP experiment (Fig. S7B) is to account for the latency in initiating an antidromic spike. (C) Example voltage responses of soma to TBP induction (B). (D) Multiple runs of somatic responses showing a train of 10 evoked EPSPs at 20 Hz on the control pathway. The waveforms illustrate the absence of robust postsynaptic summation with 20 Hz inter-pulse interval. Consequently, inter-pulse interval was set to 25 Hz for measuring evoked temporal summation (Fig. 6). Time courses of normalized $\overline{R}_{in}$ (E) and f_R (F) during TBP experiments show a reduction in input resistance and increase in resonance frequency following TBP. (G) Relationship between changes in f_R and $\overline{R}_{in}$ in TBP experiments. The R and p values correspond to the outcome of the *Pearson's* correlation test. (H) Population plots of action potential firing frequency as a function of injected current to the soma bring out significant reductions after TBP (Baseline: ●; 40 min after TBP: ●). *: $p<0.05$, paired *Student's t* test. (I) Summary plot of percentage changes in various parameters, at 40 minutes after TBP, relative to respective baseline values. After TBP, all parameters were significantly different from their respective baseline values (**R_{in}:** Baseline: 65.07 ± 4.66 MΩ; TBP: 43.34 ± 3.02 MΩ; $p<0.001$. **f_R:** Baseline: 4.53 ± 0.24 Hz; TBP: 6.21 ± 0.19 Hz, $p<0.001$. **Q:** Baseline: 1.17 ± 0.04; TBP: 1.40 ± .027; $p<0.05$. **Sag:** Baseline: 20.88 ± 1.28; TBP: 25.92 ± 1.10. $p<0.01$, paired *Student's t* test). TBP-induced depolarizing shift to resting membrane potential across the three populations was 3.26 ± 0.53 mV ($p<0.001$; paired *Student's t* test).

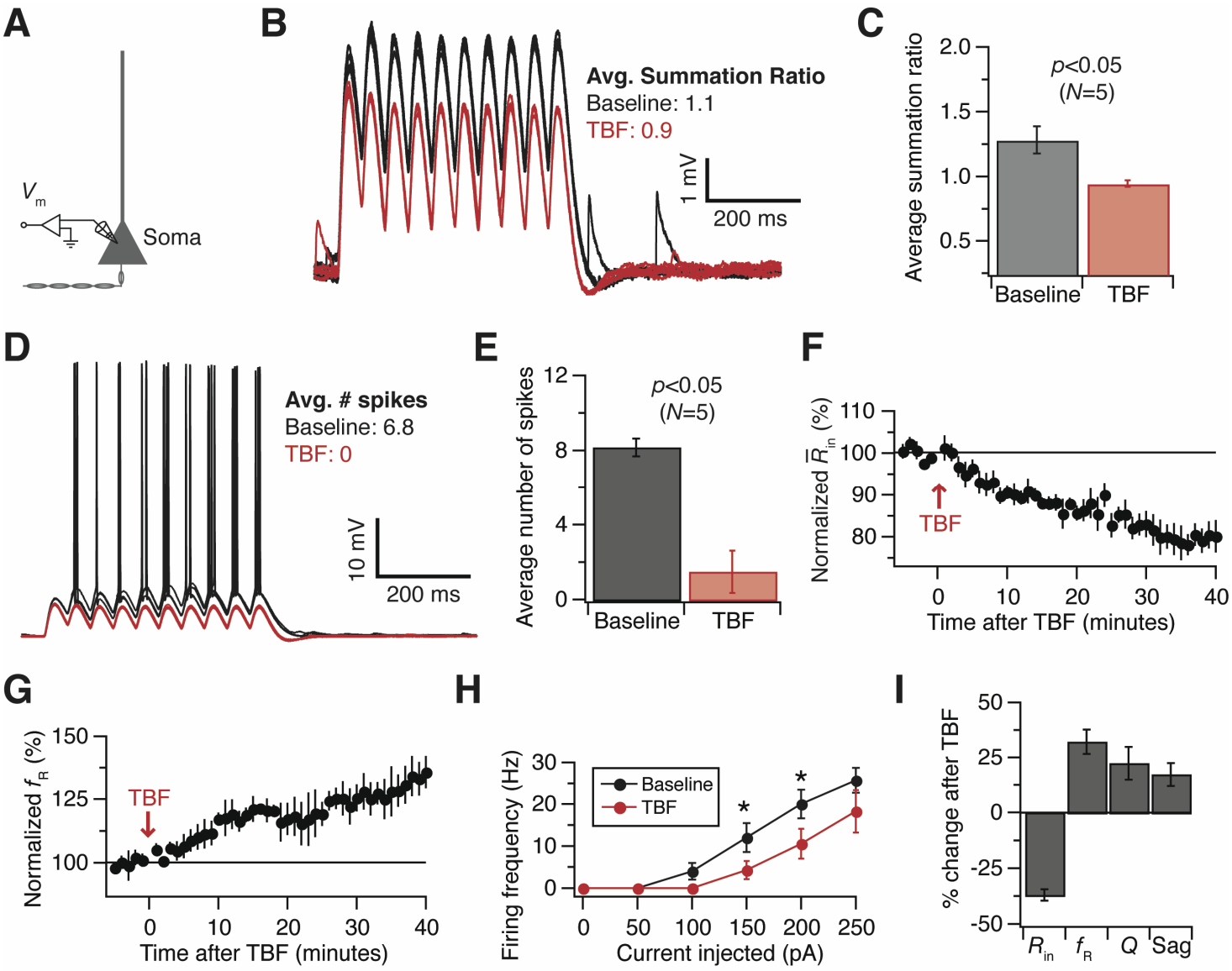
A
V_m
Soma
B
Avg. Summation Ratio
Baseline: 1.1
TBF: 0.9
1 mV
200 ms
C
Average summation ratio
2.0
1.5
1.0
0.5
p<0.05
(N=5)
Baseline
TBF
D
Avg. # spikes
Baseline: 6.8
TBF: 0
10 mV
200 ms
E
Average number of spikes
12
8
4
0
p<0.05
(N=5)
Baseline
TBF
F
Normalized $\bar{R}_{in}$ (%)
110
100
90
80
TBF
0
10
20
30
40
Time after TBF (minutes)
G
Normalized f_R (%)
150
125
100
TBF
0
10
20
30
40
Time after TBF (minutes)
H
Firing frequency (Hz)
30
20
10
0
Baseline
TBF
*
*
0
50
100
150
200
250
Current injected (pA)
I
% change after TBF
50
25
0
-25
-50
R_{in}
f_R
Q
Sag

Figure S10. (A) Schematic of the somato-apical trunk depicting the experimental design for assessing activity-dependent plasticity in temporal summation. Voltage responses of the soma were recorded using a whole-cell patch-clamp electrode (V_m). Plasticity in temporal summation, input resistance and resonance frequency are assessed following theta burst firing (TBF). (B) Multiple runs of somatic responses showing a train of 10 α-EPSPs at 20 Hz before (black) and after (red) TBF. The amplitude of current injection was the same before and after TBF. TBF-induced reduction in temporal summation may be observed by comparing the amplitudes of first and last EPSPs in the train. (C) Population plot of average summation ratio before and 40 minutes after TBF illustrate a significant reduction (paired *Student's t* test) in temporal summation following TBF. (D) Multiple runs of somatic responses showing a train of 10 α-EPSPs at 20 Hz before (black) and after (red) TBF. This example is obtained from the same cell as the one shown in (B). The amplitude of current injection was higher than that shown in (B) in order to able to induce spikes, and was the same before and after TBF. A clear reduction in number of spikes may be noted following TBF. (E) Population plot of average number of spikes before and 40 minutes after TBF illustrate a significant reduction (paired *Student's t* test) in temporal summation induced spikes following TBF. Time courses of normalized $\overline{R}_{in}$ (F) and f_R (G) during TBF experiments show a reduction in input resistance and an increase in resonance frequency following TBF. (H) Population plots of action potential firing frequency as a function of injected current to the soma bring out significant reductions after TBF (Baseline: ●; 40 min after TBF: ●). *: $p<0.05$, paired *Student's t* test. (I) Summary plot of percentage changes in various parameters, at 40 minutes after TBP, relative to respective baseline values. After TBF, all parameters are significantly different from their respective baseline values (**R_{in}:** Baseline: 88.25 ± 8.82 MΩ; TBF: 55.63 ± 5.99 MΩ; $p<0.01$. **f_R:** Baseline: 4.73 ± 0.24 Hz; TBF: 6.16 ± 0.20 Hz, $p<0.01$. **Q:** Baseline: 1.13 ± 0.02; TBF: 1.32 ± 0.06; $p<0.05$. **Sag:** Baseline: 19.84 ± 0.92; TBF: 24.21 ± 1.59. $p<0.05$, paired *Student's t* test). TBF-induced depolarizing shift to resting membrane potential was 3.73 ± 0.77 mV ($p<0.001$; paired *Student's t* test).

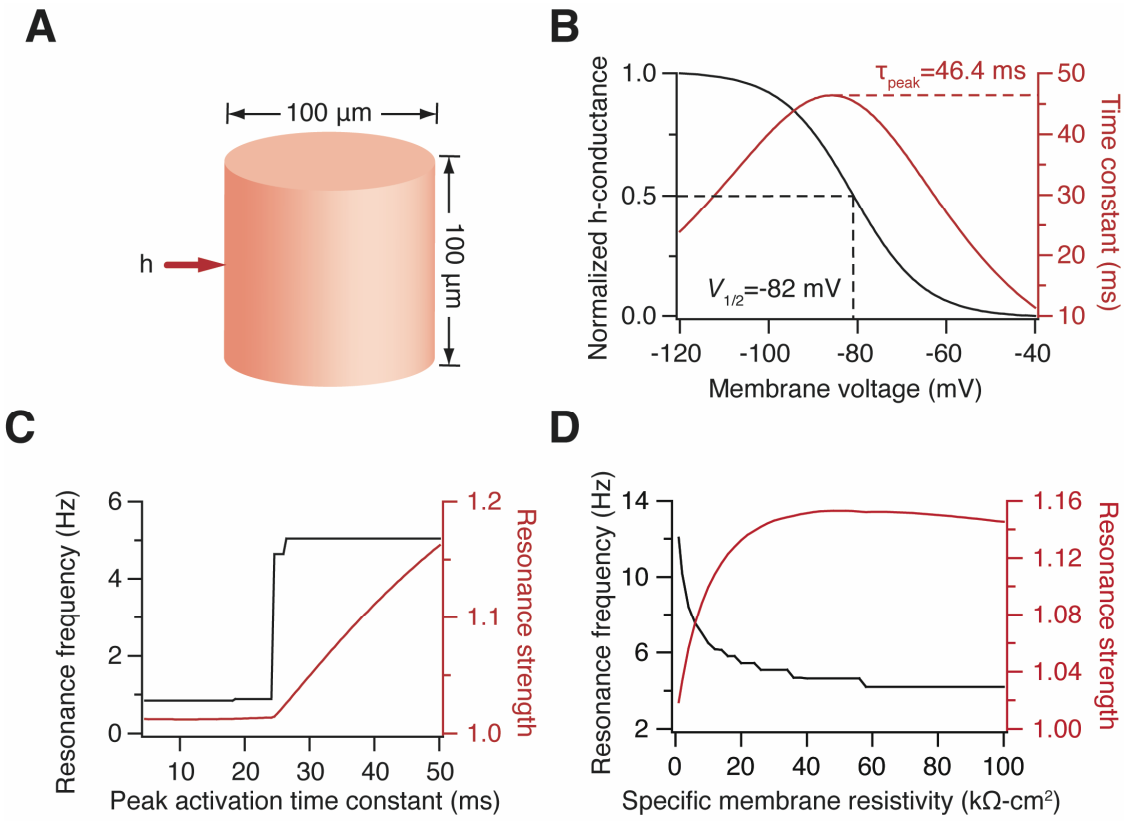
A
100 µm
100 µm
h
B
Normalized h-conductance
1.0
0.5
0.0
τpeak=46.4 ms
V1/2=-82 mV
50
40
30
20
10
Time constant (ms)
-120
-100
-80
-60
-40
Membrane voltage (mV)
C
Resonance frequency (Hz)
6
4
2
0
1.2
1.1
1.0
Resonance strength
10
20
30
40
50
Peak activation time constant (ms)
D
Resonance frequency (Hz)
14
10
6
2
1.16
1.12
1.08
1.04
1.00
Resonance strength
0
20
40
60
80
100
Specific membrane resistivity (kΩ-cm²)

Figure S11. (A) Schematic of the single compartment model used in obtaining the outcomes shown in Fig. 7 and in (C). The only active current in the model is I_h. (B) Activation curve (black) and activation/deactivation time constant (red) of the *h*-conductance used in the model. (C) Experimental value of peak activation time constant of *h*-channels, τ_{peak}, is 46.4 ms (B; Magee, 1998). Systematically varying τ_{peak}, and scaling the activation time constant curve (red in (B)) to this peak value, to obtain the resonance frequency and resonance strength of the single compartment model (Fig. 7) confirms the requirement that sustenance of resonance requires the activation time constant to be higher than a certain threshold (Hutcheon et al., 1996; Hutcheon and Yarom, 2002). It may be observed that until a threshold value (threshold τ_{peak}=24.5 ms in this case), resonance frequency and resonance strength are close to unity, confirming that resonance is abolished below the threshold value. Beyond this threshold value, resonance frequency jumps and stays at a given resonance frequency value, while resonance strength increases linearly. This threshold value is largely dependent on the cell's membrane time constant (Hutcheon et al., 1996). These simulations were performed at -65 mV, with other parameters set as in (Fig. 7D). (D) Resonance frequency decreases and resonance strength increases with increase in specific membrane resisitivity, R_m (Hutcheon et al., 1996). Even though resonance frequency can be increased through reduction in R_m (or equivalently increase in leak conductance), both distance- (Fig. 1) and activity-dependent (Fig. 3–6) increases in resonance frequency are due to increase in I_h because resonance strength (Q) increases in both cases. This increase in Q is consistent with increase in I_h (Fig. 7C), and not with a reduction in R_m. Further, such I_h-independent changes in conductance across distance appear to be insignificant both in input resistance measurements (Fig. 2F–G), and in the impedance amplitude profile measurements (*e.g.,* Fig. S3B) performed in ZD7288 treated slices, thus ruling out the possibility that the distance-dependent increase in resonance frequency is due to an increase in a leak conductance. Finally, an increase in a leak conductance would manifest itself as a reduction in impedance amplitude at all frequencies (Hutcheon et al., 1996), while increase in I_h manifests itself as a reduction in impedance amplitude specifically at lower frequencies (Fig. 7B). Following activity-dependent plasticity, impedance amplitude reduces specifically at lower frequencies (Fig. 3C; Fig. S7G), thus strongly suggesting an increase in I_h underlying activity-dependent plasticity in f_R.

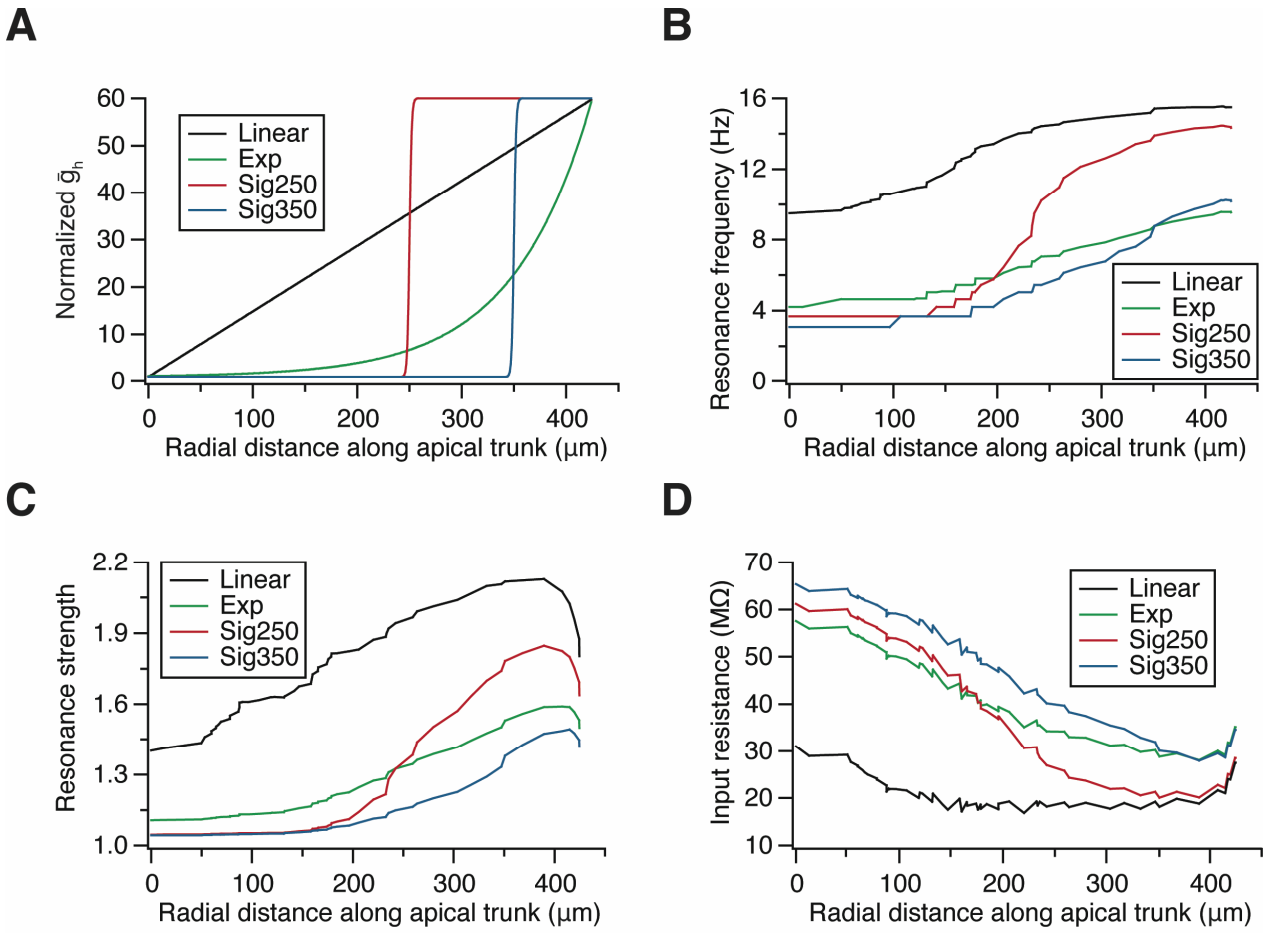
A
Normalized $\bar{g}_h$
60
50
40
30
20
10
0
0
100
200
300
400
Radial distance along apical trunk (µm)
Linear
Exp
Sig250
Sig350
B
Resonance frequency (Hz)
16
12
8
4
0
0
100
200
300
400
Radial distance along apical trunk (µm)
Linear
Exp
Sig250
Sig350
C
Resonance strength
2.2
1.9
1.6
1.3
1.0
0
100
200
300
400
Radial distance along apical trunk (µm)
Linear
Exp
Sig250
Sig350
D
Input resistance (MΩ)
70
60
50
40
30
20
10
0
100
200
300
400
Radial distance along apical trunk (µm)
Linear
Exp
Sig250
Sig350

Figure S12. Analysis of the effect of various profiles of $\bar{g}_h$, as a function of radial distance from the soma, on resonance properties and input resistance. (A) Various profiles of $\bar{g}_h$ as a function of radial distance from the soma. The neuronal projection shown in Fig. 8A was used for these multicompartmental simulations. All the profiles were designed such that $\bar{g}_h$ at a distal dendrite is 60 times higher than $\bar{g}_h$ at the soma (in conformation with Lorincz et al., 2002). The absolute values of density at the soma (34 μS/cm^2) and at the most distal point (2.04 mS/cm^2) on the tree were kept the same across all profiles. The exponential function (Exp) has a τ of 75 μm, corresponding to that obtained from the resonance frequency vs. distance plot (Fig. 2C). Sig250 and Sig350 correspond to sigmoids with $x_{1/2}$ at 250 μm and 350 μm, respectively. Profiles of local resonance frequency (B), local resonance strength (C) and local input resistance (D) along the somato-apical trunk, as functions of radial distance from the soma, are shown for each of the cases depicted in (A). It may be noted that a linear increase in *h*-channel density is unable to match experimental data. While the exact values of parameters may vary, these simulations indicate that a sharp increase of *h*-channel density in distal dendrites is required to match experimental observations (Fig. 1), consistent with observations made by (Lorincz et al., 2002). This, along with the fact that there is an increase in *h*-channel density within the stratum radiatum (Lorincz et al., 2002; Magee, 1998) led us to use the profile shown in Fig. 8B. Finally, even though the density of *h*-channels in the soma is the same across all profiles in (A), the measured parameter values at the soma are different (B–D) for each of the profiles. This is reflective of contributions from *h*-channels in other compartments, in a distance-dependent manner, which is also reflected in Fig. 8 and in Figs. S13–S14.

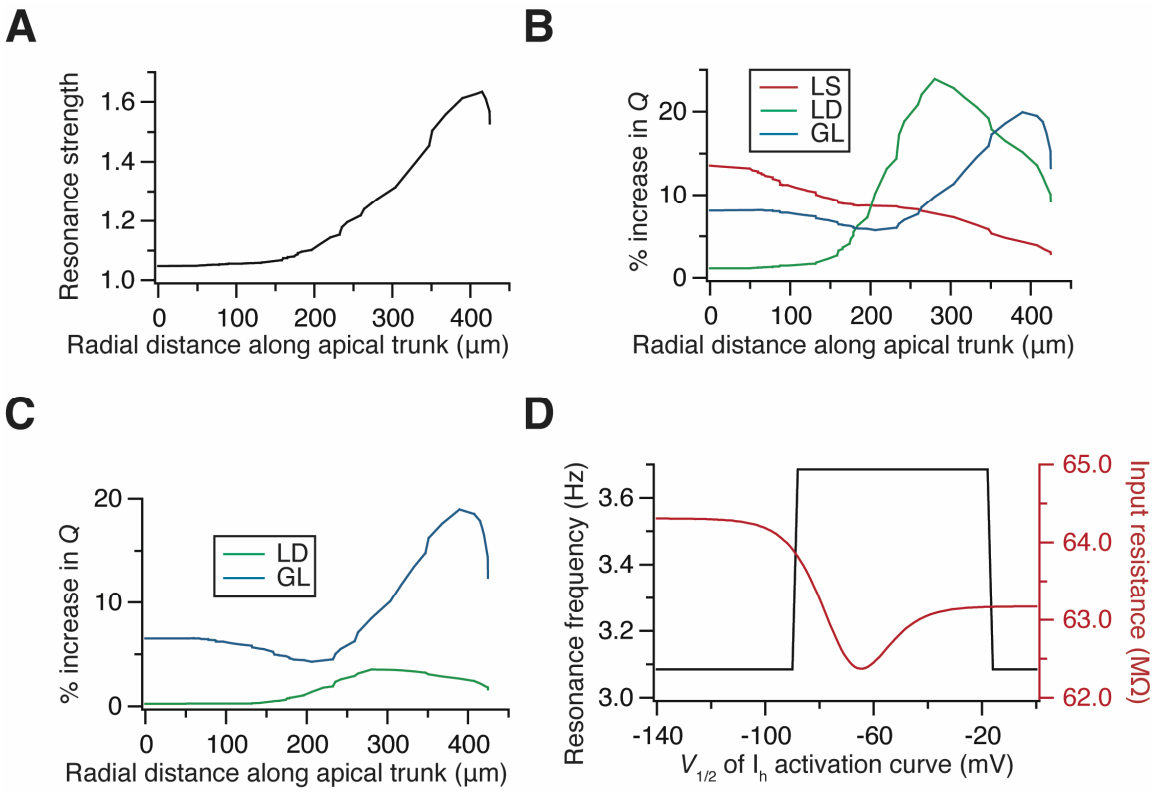
A
Resonance strength
1.6
1.4
1.2
1.0
0
100
200
300
400
Radial distance along apical trunk (µm)
B
% increase in Q
20
10
0
LS
LD
GL
0
100
200
300
400
Radial distance along apical trunk (µm)
C
% increase in Q
20
10
0
LD
GL
0
100
200
300
400
Radial distance along apical trunk (µm)
D
Resonance frequency (Hz)
3.6
3.4
3.2
3.0
65.0
64.0
63.0
62.0
Input resistance (MΩ)
-140
-100
-60
-20
V1/2 of Ih activation curve (mV)

Figure S13. (A) Profile of local resonance strength (Q) along the somato-apical trunk as a function of radial distance from the soma in the model cell shown in Fig. 8A. The profile of h-conductance across the dendritic tree is set as in Fig. 8B. (B)–(C) Irrespective of whether increase in I_h is due to increase in maximal conductance (B) or depolarizing shift of activation kinetics (C), a global increase in I_h (GL; Fig. 8D) is required to match experimental results on near-identical increase in resonance strength (Fig. 4 and Fig. 5) across the dendritic tree. It may be noted that while increase in I_h confined to soma leads to local changes only around the soma (B; LS), increase in I_h confined to a dendritic segment leads to local changes only around that segment (B and C; LD). (D) Input resistance (red) and resonance frequency (black) plotted as functions of local *somatic* $V_{1/2}$ of the I_h activation curve. This demonstrates that changing somatic $V_{1/2}$ of I_h activation curve alone (LS case in Fig. 8H–8J) cannot significantly increase resonance frequency or significantly decrease input resistance from the baseline value ($V_{1/2}$=-82 mV).

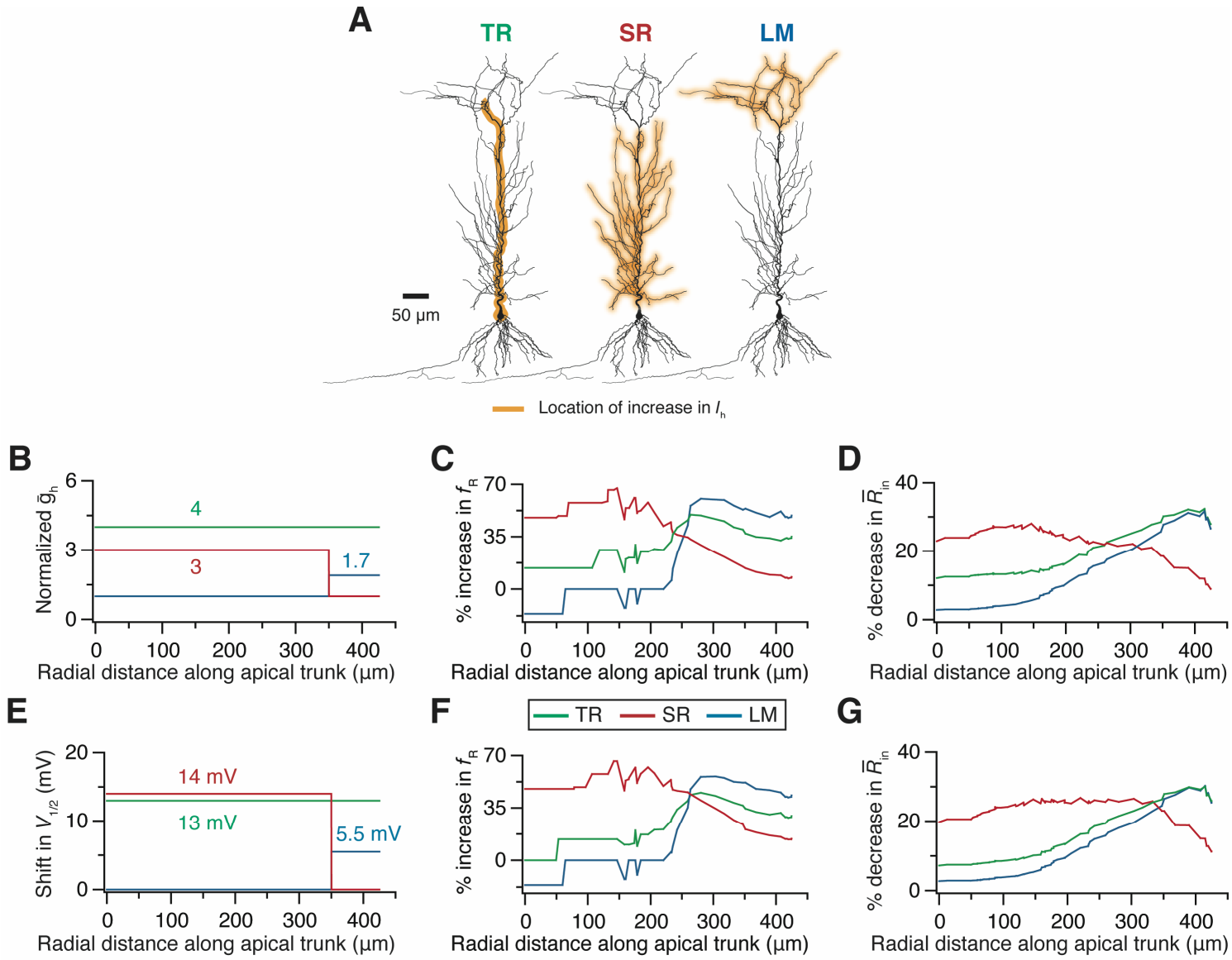
A
TR
SR
LM
50 µm
Location of increase in I_h
B
Normalized $\bar{g}_h$
4
3
1.7
Radial distance along apical trunk (µm)
C
% increase in f_R
Radial distance along apical trunk (µm)
D
% decrease in $\bar{R}_{in}$
Radial distance along apical trunk (µm)
E
Shift in $V_{1/2}$ (mV)
14 mV
13 mV
5.5 mV
Radial distance along apical trunk (µm)
F
TR
SR
LM
% increase in f_R
Radial distance along apical trunk (µm)
G
% decrease in $\bar{R}_{in}$
Radial distance along apical trunk (µm)

Figure S14. (A) Graphical illustration of the three different possibilities tested with simulations on the location of increase in I_h. Left: expression of plasticity is confined to the apical trunk (TR); middle: expression of plasticity confined to the dendrites in stratum radiatum (SR); right: expression of plasticity confined to the dendrites in stratum lacunosum moleculare (LM). Color-codes of the labels on the top of each neuron serve for interpretation of plots in (B)–(G). We increase I_h by either increasing maximal *h*-conductance, $\bar{g}_h$, or by depolarizing $V_{1/2}$ of the I_h activation curve. Under each of these two cases, we assess the effects of increasing I_h as specified by the three possible configurations in (A) (TR, SR and LM). We increase I_h such that the maximal percentage change in input resistance is around 25–30% for each of the three cases. The exact profile of changes required in $\bar{g}_h$ ((B); values of $\bar{g}_h$ are normalized with respect to the baseline profile in Fig. 8B) or $V_{1/2}$ ((E); values indicate depolarizing shifts to the activation kinetics with respect to baseline values) are shown for each of the three configurations in (A) (TR, SR and LM). Increasing $\bar{g}_h$ across the apical trunk (TR) matches experimental results (Fig. 4–5) on near-identical plasticity in resonance frequency (C) and input resistance (D; not as clearly as resonance frequency matches) across the apical trunk. However, shifting the activation kinetics across the apical trunk (TR) is not able to match experimental results (F) & (G), especially in the proximal regions and the soma (owing to the bell-shaped dependence of resonance frequency on $V_{1/2}$; Fig. 7D). Irrespective of whether increase in I_h was effectuated through change in $\bar{g}_h$ (C) & (D) or $V_{1/2}$ (F–G), increase in I_h is confined to stratum radiatum (SR) or stratum lacunosum moleculare (LM) leads to local changes only around those respective subregions. It may also be noted that change in I_h need not be at the soma for changes in resonance frequency ((C) & (F); SR) and input resistance ((D) & (G); SR) to be measured at the soma.